

## Supporting Information

### Exclusive Ni-N<sub>4</sub> Sites Realize Near-unity CO Selectivity for

#### Electrochemical CO<sub>2</sub> Reduction

Xiaogang Li<sup>1†</sup>, Wentuan Bi<sup>1†</sup>, Minglong Chen<sup>2†</sup>, Yuexiang Sun<sup>1</sup>, Huanxin Ju<sup>3</sup>, Wensheng Yan<sup>3</sup>, Junfa Zhu<sup>3</sup>, Xiaojun Wu<sup>2</sup>, Wangsheng Chu<sup>3</sup>, Changzheng Wu<sup>1\*</sup>, and Yi Xie<sup>1</sup>

1. Hefei National Laboratory for Physical Sciences at the Microscale, iChEM (Collaborative Innovation Center of Chemistry for Energy Materials), and CAS Key Laboratory of Mechanical Behavior and Design of Materials, University of Science and Technology of China, Hefei 230026, P.R. China.
2. CAS Key Lab of Materials for Energy Conversion, Department of Materials Science and Engineering, University of Science and Technology of China, Hefei 230026, P.R. China
3. National Synchrotron Radiation Laboratory, University of Science and Technology of China, Hefei, Anhui 230026, China.

† These authors contributed equally to this work

To whom correspondence should be addressed E-mail: czwu@ustc.edu.cn.

## Catalyst preparation

### *Synthesis of Ni-doped g-C<sub>3</sub>N<sub>4</sub>*

2 g of dicyandiamide, 10 g of NH<sub>4</sub>Cl and NiCl<sub>2</sub> with various addition (0.1 mmol, 0.2 mmol, 0.3 mmol and 0.4 mmol respectively) were dissolved in 30 ml deionized water followed by freeze-drying. Then, 4 g of freeze-dried powder was placed in a crucible and heated at 550 °C for 2 h at a rate of 5 °C min<sup>-1</sup>. The synthesis of blank g-C<sub>3</sub>N<sub>4</sub> is the same as that of Ni-doped g-C<sub>3</sub>N<sub>4</sub> except the addition of NiCl<sub>2</sub>.

### *Synthesis of Ni-N<sub>4</sub>-C, N-C, Ni@N-C and Ni@N-C-Glu*

For the synthesis of **Ni-N<sub>4</sub>-C**, 0.5 g Ni-doped g-C<sub>3</sub>N<sub>4</sub> were dispersed in 35 ml 0.03 M glucose solution under sonication for 4 h. Then the above mixture was transferred into a 40 ml Teflon-lined autoclave, sealed and heated at 180 °C for 10 h. The final product after cleaning and drying then was annealed at 1000 °C in Ar atmosphere for 1 h. The synthesis of **N-C** followed the same process with the blank g-C<sub>3</sub>N<sub>4</sub> substituting Ni-doped g-C<sub>3</sub>N<sub>4</sub>. The direct pyrolysis of Ni-doped g-C<sub>3</sub>N<sub>4</sub> at 1000 °C in Ar atmosphere for 1 h leads to the formation of **Ni@N-C**. For the synthesis of **Ni@N-C-Glu**, the mixture of glucose and the precursor for Ni-doped g-C<sub>3</sub>N<sub>4</sub> after freeze-drying placed in a crucible and heated at 550 °C for 2 h at a rate of 5 °C min<sup>-1</sup>. The cooled product then was annealed at 1000 °C in Ar atmosphere for 1 h.

### *Characterization*

Transmission electron microscopy (TEM) images were taken on H-7700 (Hitachi, Japan) operated at an acceleration voltage of 100 kV. The X-ray powder diffraction (XRD) was conducted by a Philips X'Pert Pro Super diffractometer equipped with graphite monochromatized Cu-K $\alpha$  radiation ( $\lambda = 1.54178 \text{ \AA}$ ). The high-angle annular dark-field scanning transmission electron microscopy (HAADF-STEM) characterization was performed on a JEOL JEM-ARF200F TEM/STEM with a spherical aberration corrector. Raman spectra were recorded at ambient temperature with LABRAM-HR Confocal Laser Micro Raman Spectrometer 750 K with a laser power of 0.5 mW. The loading of Ni was measured on inductively coupled plasma-atomic emission spectrometer (ICP-AES) on an Optima 7300 DV (PerkinElmer Corporation). X-ray photoelectron spectroscopy (XPS) measurements and XAS for N and C K-edge were performed at the Catalysis and Surface Science End station at the BL11U beamline in the National Synchrotron Radiation Laboratory (NSRL) in Hefei, China. Ni L-edge soft X-ray absorption spectroscopy (XAS) was performed at the beamline BL12b of national synchrotron radiation laboratory (NSRL, Hefei) in the total electron yield (TEY) mode by collecting the sample drain current under a vacuum better than 10<sup>-7</sup> Pa. The Ni K-edge XAS data were collected at the beamline 1W1B of the Beijing Synchrotron Radiation Facility (BSRF, Beijing) in the fluorescence mode using a Lytle detector.

### *Electrochemical measurements*

Electrochemical measurements were carried out in a three-electrode system at an electrochemical station (CHI760E). The working electrode was prepared by the following process: 10  $\mu$ l ink, prepared by dispersing 4  $\mu$ g sample and 60  $\mu$ l Nafion solution into 0.94 ml ethanol solution, was loaded on onto a glassy carbon electrode with 5 mm diameter. The Ag/AgCl

electrode and graphite serve as reference and counter electrodes. LSV test was performed in CO<sub>2</sub>-saturated 0.5 M KHCO<sub>3</sub> solution with a scan rate of 20 mV/s. ECSA referred the CV results under the potential windows of -0.4 V~-0.5 V (vs Ag/AgCl). Electrochemical impedance spectroscopy (EIS) measurements were carried out by applying an AC voltage with 5 mV amplitude in a frequency range from 100 KHz to 100 mHz. For the faradaic efficiency analysis, gas products were detected by gas chromatograph (Agilent 7890B) and liquid product was characterized by <sup>1</sup>H NMR on Bruker AVANCE AV III 400.

### ***Computational Details***

Our calculations were carried out with use of spin-polarized periodic density functional theory (DFT) implemented in Vienna ab initio simulation package (VASP)<sup>1</sup>. The electron-ion interactions were described by the projector augmented wave (PAW) method<sup>2</sup> and the electron exchange and correlation energy were coped with the gradient corrected Perdew-Burke-Ernzerh of (GGA-PBE)<sup>3</sup> functional. The kinetic cutoff energy for plane-wave basis set was set as 500 eV. For geometric optimization, the total energy convergence was set to be smaller than 10<sup>-5</sup> eV, and the force convergence was set to be lower than 0.02 eV/Å on atoms during optimization. Electron smearing of  $\sigma=0.02$  eV was used following the Gaussian scheme. Brillouin zone sampling was employed using a Monkhorst-Packing grid 5×5×1.<sup>4</sup> Dispersion corrections have been taken care of by incorporating Grimme's<sup>5</sup> atom-pairwise dispersion correction approach (DFT+D3) as implemented in VASP. The solvation effects was not considered in the simulations. The 5×5 supercell of graphene doped by nickel and nitrogen is applied in this model. Besides, Ni<sub>4</sub> cluster loaded on Nitrogen-doped graphene as model for Ni@N-C and Ni@N-C-Glu were also constructed. The aperiodic directions have a 20 Å cell spacing to eliminate the interaction of periodic images of the system. The ground state structures of COOH\*, CO\* and H\* adsorbed on Ni-N<sub>4</sub>-C, N-C and Ni<sub>4</sub> cluster were determined by testing all the possible configurations on possible active sites and found the lowest energy one. The chemical potential of H<sub>2</sub> (g) is equivalent to that of  $\mu$  (H<sup>+</sup>+e<sup>-</sup>)=1/2 $\mu$  (H<sub>2</sub>). The free energy for adsorbates and non-adsorbed gas-phase molecules is calculated as  $\Delta G = \Delta E_{\text{elec}} + \Delta E_{\text{ZPE}} - T\Delta S + \int C_p dT$ ,<sup>6</sup> where T is the temperature, E<sub>elec</sub> is the electronic energy calculated by DFT; E<sub>ZPE</sub> is the zero point energy estimated under harmonic approximation by taking the vibrational frequencies of adsorbates or molecules as calculated within DFT. Moreover the entropies of free gases were just considered from the NIST database, and the adsorbed species were only taken vibrational entropy into account. The  $\int C_p dT$  is small for the adsorbates compared to E<sub>elec</sub> and E<sub>ZPE</sub>, and thus neglected in this study for adsorbates. We define the difference of free energy  $\Delta G = \Delta G_0$  at 0 V RHE, and in general,  $\Delta G(U) = \Delta G_0 + eU$ .

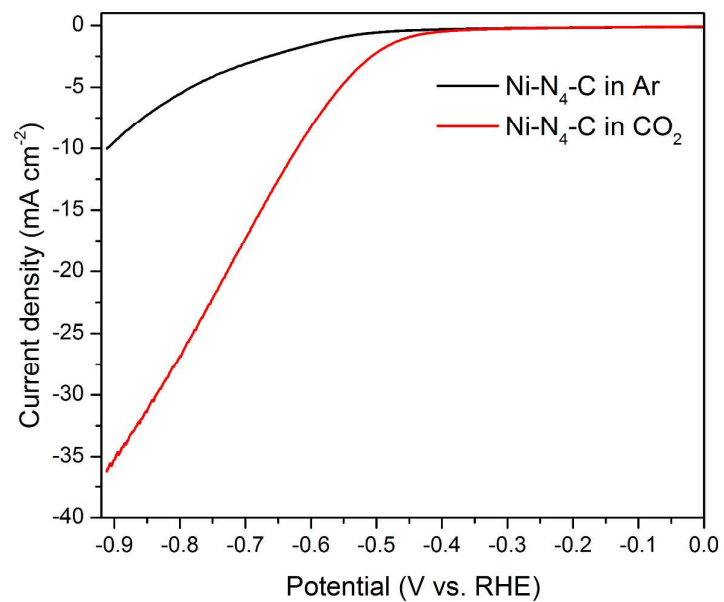


**Figure S1. Linear sweep voltammetric curves of Ni-N<sub>4</sub>-C in Ar-saturated and CO<sub>2</sub>-saturated 0.5 M KHCO<sub>3</sub> aqueous solution.**

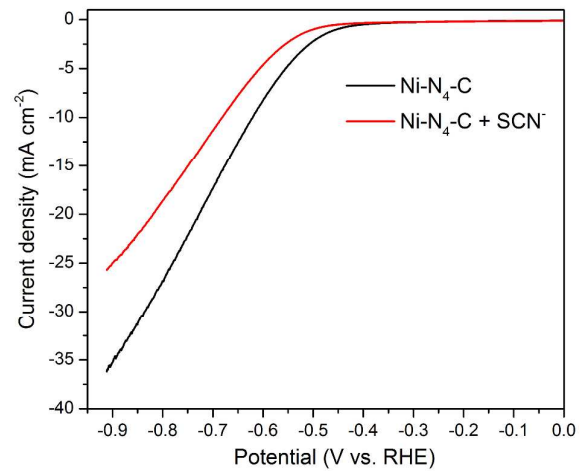


**Figure S2. Linear sweep voltammetric curves of Ni-N<sub>4</sub>-C and Ni-N<sub>4</sub>-C with 0.02 M KSCN.**

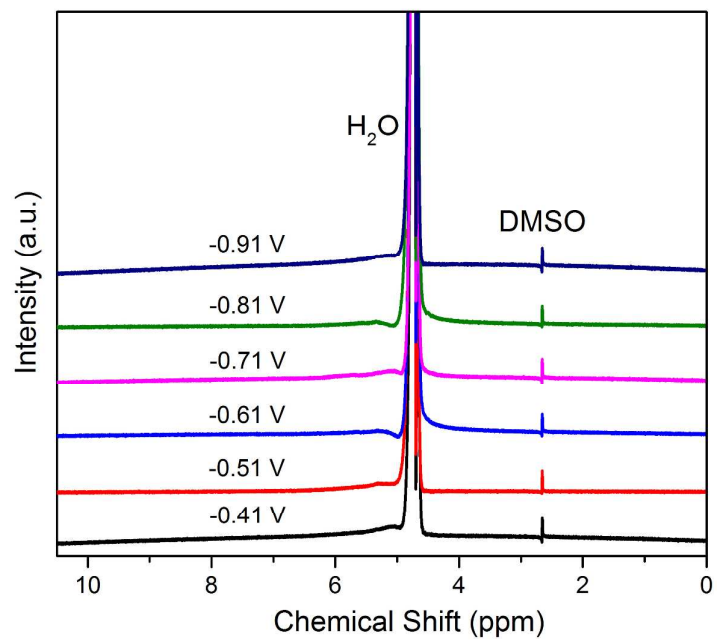


**Figure S3. Characterization for the liquid product of Ni-N<sub>4</sub>-C during 2-h CO<sub>2</sub> reduction process by  $^1\text{H}$  nuclear magnetic resonance spectroscopy.**

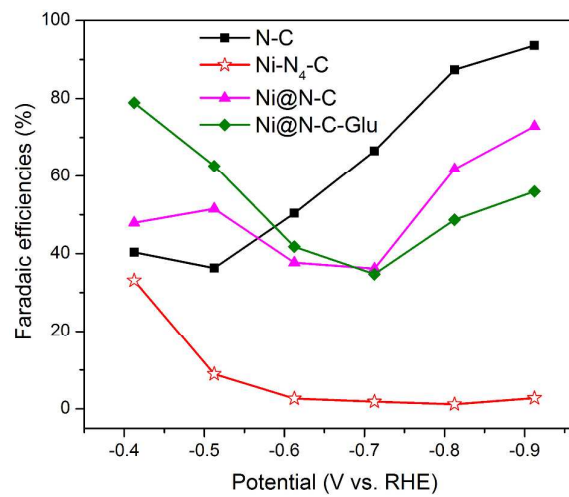


**Figure S4. Faradaic efficiencies for H<sub>2</sub>.**

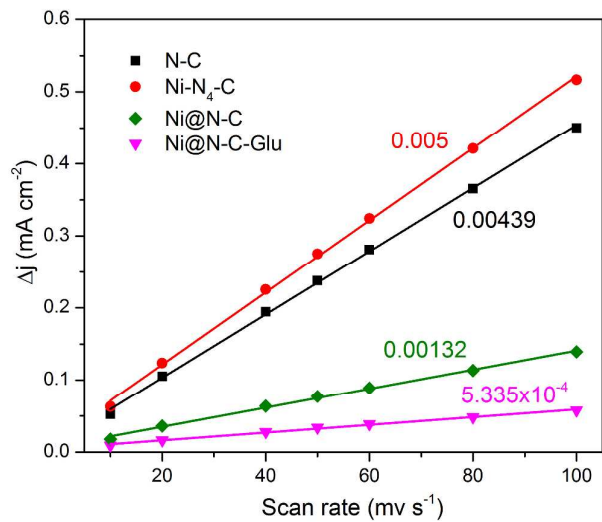
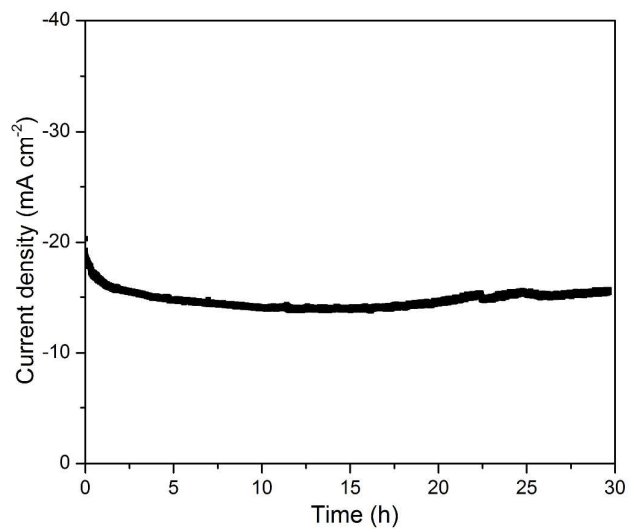
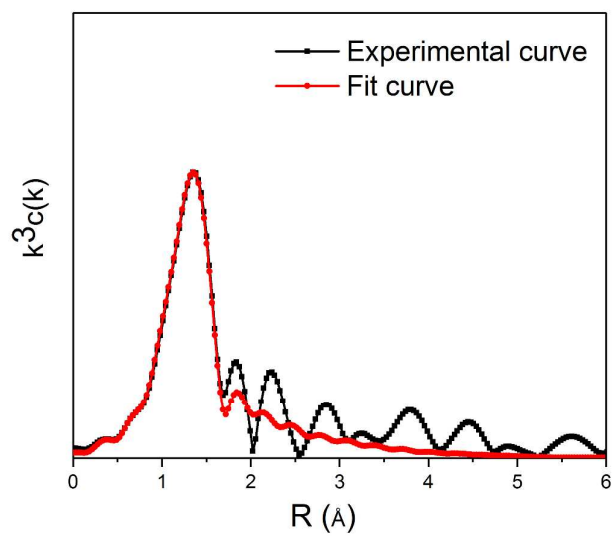


Figure S5. Charging current density differences plotted against scan rates.



**Figure S6. Chrono-Amperometry results for Ni-N<sub>4</sub>-C at the potentials of -0.81 V vs RHE.**



**Figure S7. Comparison of FT-EXAFS curves between the experimental data and the fit of the Ni-N<sub>4</sub>-C.**

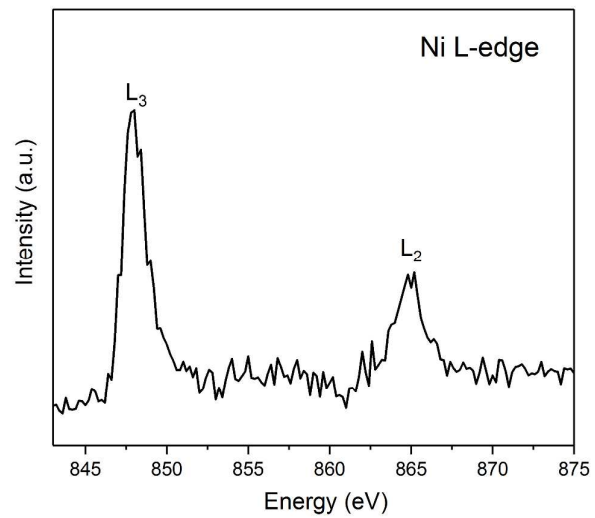


**Figure S8. Ni L-edge XAS spectra of Ni-N<sub>4</sub>-C.**

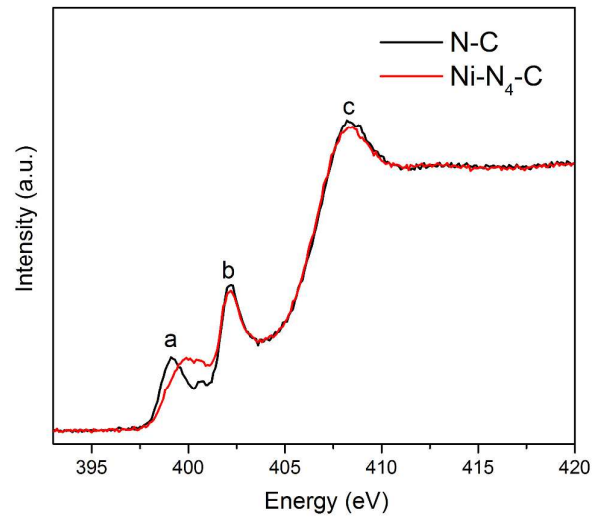


**Figure S9. N K-edge XAS of Ni-N<sub>4</sub>-C and N-C.**

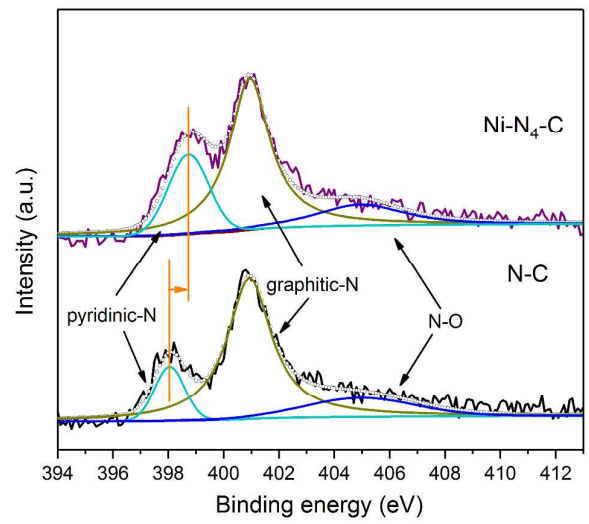


**Figure S10.** N 1s XPS spectra of Ni-N<sub>4</sub>-C and N-C.

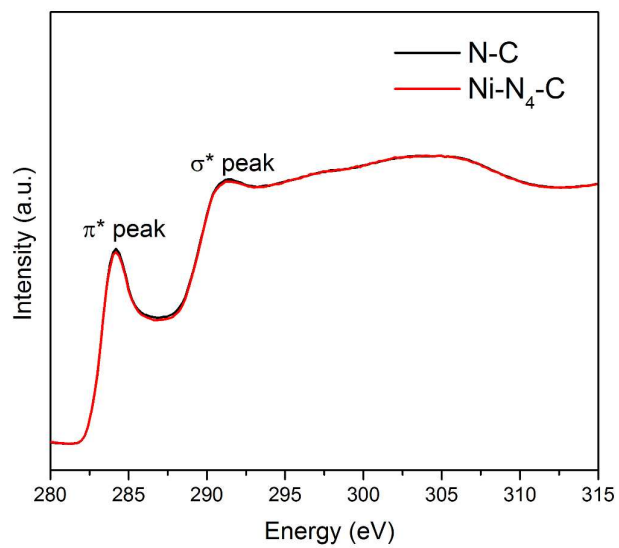


**Figure S11. C K-edge XAS of Ni-N<sub>4</sub>-C and N-C.**

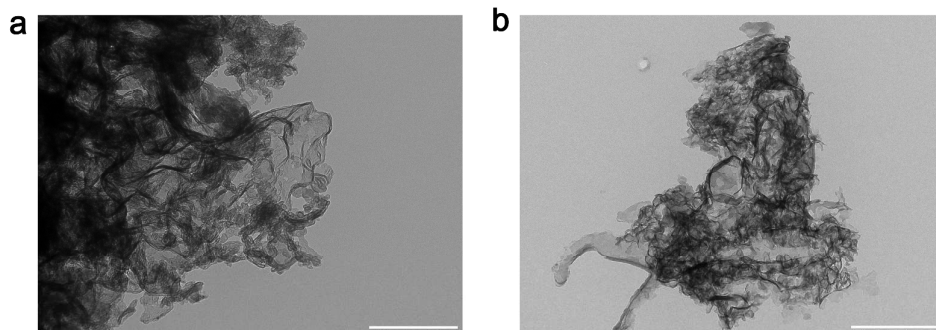


**Figure S12. TEM images of N-C (a) and Ni-doped g-C<sub>3</sub>N<sub>4</sub> (b).**

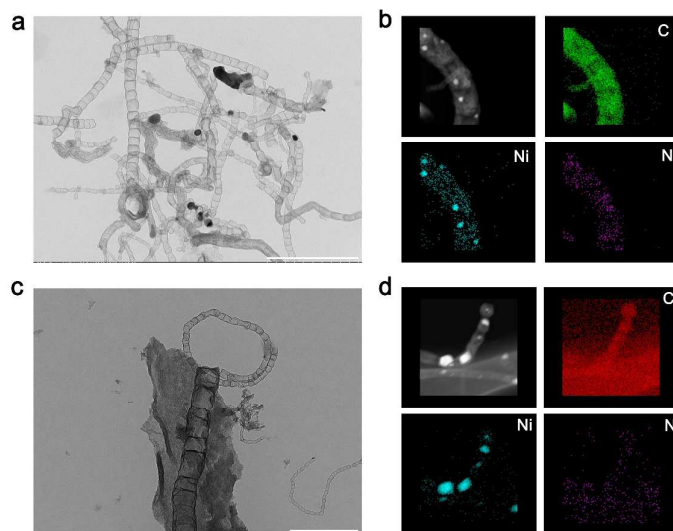


**Figure S13. (a) TEM image of Ni@N-C. (b) Element mapping image of Ni@N-C. (c) TEM image of Ni@N-C-Glu. (d) Element mapping image of Ni@N-C-Glu. Scale bar is 500 nm.**

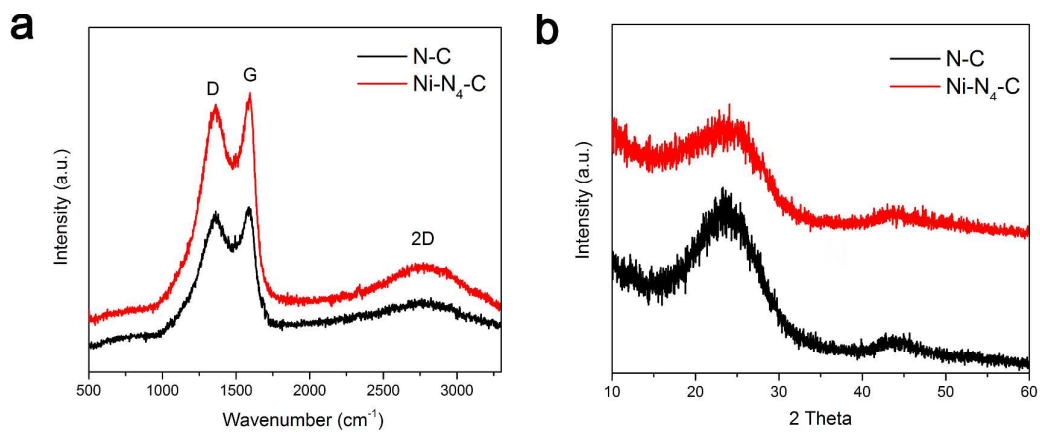


**Figure S14.** (a) Raman spectrums of Ni-N<sub>4</sub>-C and N-C. (b) XRD patterns of Ni-N<sub>4</sub>-C and N-C.

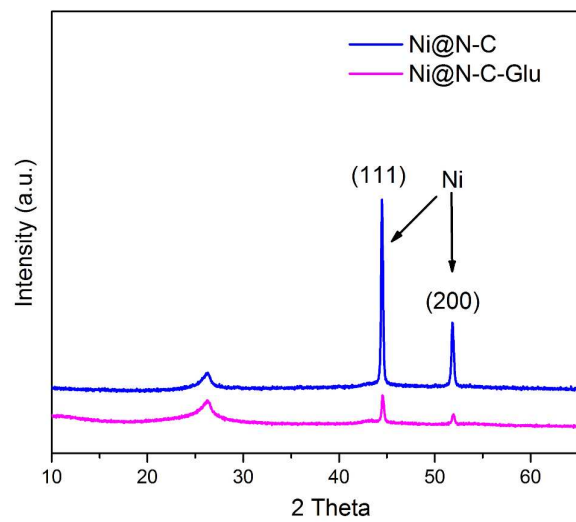


**Figure S15.** XRD patterns of Ni@N-C and Ni@N-C-Glu.

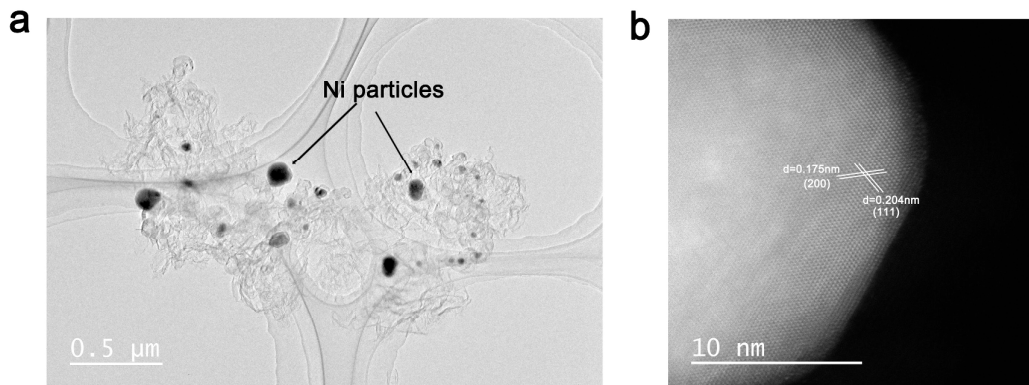


**Figure S16.** TEM image (a) and HAADF-STEM image (b) of Ni-N<sub>4</sub>-C with more loading of Ni (the addition of 0.4 mmol NiCl<sub>2</sub> in the synthetic process) when Ni particles begin to form.

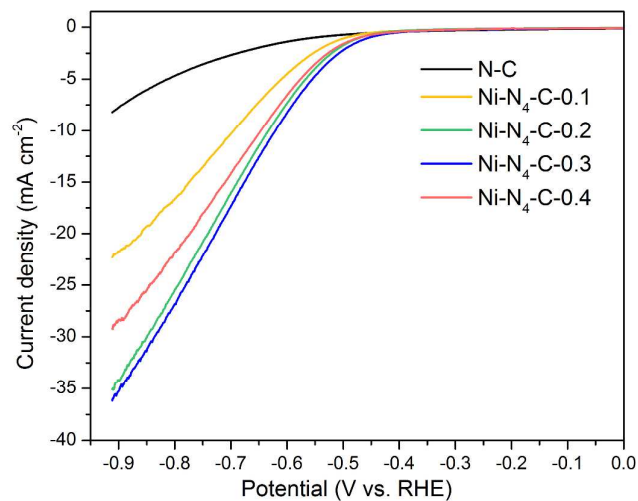


**Figure S17. Linear sweep voltammetric curves of Ni-N<sub>4</sub>-C with various Ni loading, in which 0.1, 0.2, 0.3 and 0.4 mean the mmol-addition of NiCl<sub>2</sub> in the synthetic process. The addition of 0.4 mmol NiCl<sub>2</sub> leads to the formation of Ni particles in Ni-N<sub>4</sub>-C. The characterizations for Ni-N<sub>4</sub>-C are based the sample with 0.3 mmol NiCl<sub>2</sub> addition.**

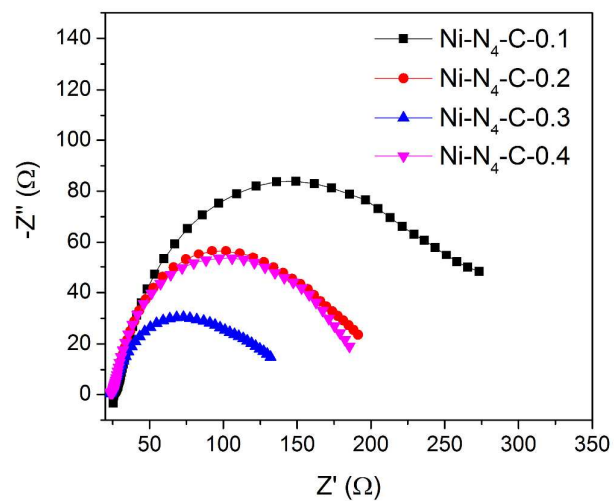


**Figure S18.** Nyquist plots of Ni-N<sub>4</sub>-C with various Ni loading.

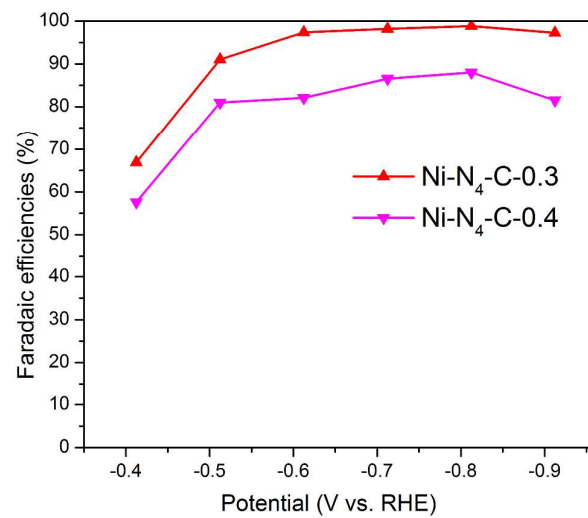


**Figure S19.** Faradaic efficiencies for CO of Ni-N<sub>4</sub>-C with 0.3 and 0.4 mmol Ni addition.

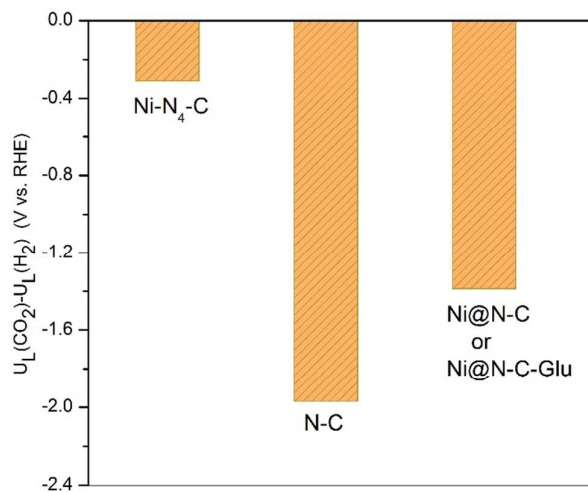


**Figure S20.** The difference in limiting potentials for CO<sub>2</sub> reduction and H<sub>2</sub> evolution of N-C, Ni-N<sub>4</sub>-C and Ni@N-C/Ni@N-C-Glu.

**Table S1. Fit results of EXAFS for Ni-doped g-C<sub>3</sub>N<sub>4</sub> and Ni-N<sub>4</sub>-C by the IFEFFIT code.**

	<i>pair</i>	<i>N</i>	<i>R</i> (Å)	$\sigma^2$ ( $\times 10^{-3} \text{Å}^2$ )	<i>E</i> <sub>0</sub> (eV)
Ni-doped g-C <sub>3</sub> N <sub>4</sub>	Ni-O	2.0	1.95 ± 0.02	11.0 ± 1.2	-8.0
	Ni-N	4.0	2.09 ± 0.02	6.2 ± 0.6	-6.0
Ni-N <sub>4</sub> -C	Ni-N	4.0 ± 0.5	1.86 ± 0.02	7.3 ± 0.7	-6.0

### **References**

1. Kresse, G.; Furthmüller, J. *Computational materials science* **1996**, *6*, 15.
2. Mortensen, J. J.; Hansen, L. B.; Jacobsen, K. W. *Phys. Rev. B* **2005**, *71*, 035109.
3. Perdew, J. P.; Burke, K.; Ernzerhof, M. *Phys. Rev. Lett.* **1996**, *77*, 3865.
4. Monkhorst, H. J.; Pack, J. D. *Phys. Rev. B* **1976**, *13*, 5188.
5. Grimme, S.; Antony, J.; Ehrlich, S.; Krieg, H. *J. Chem. Phys.* **2010**, *132*, 154104.